OCT Angiography and Cone Photoreceptor Imaging in Geographic Atrophy

Jia Qin,[1] Nicholas Rinella,[1] Qinqin Zhang,[2] Hao Zhou,[2] Jessica Wong,[1] Michael Deiner,[1] Austin Roorda,[3] Travis C. Porco,[1,4] Ruikang K. Wang,[2] Daniel M. Schwartz,[1] and Jacque L. Duncan[1]

[1]Department of Ophthalmology, University of California, San Francisco, California, United States
[2]Department of Bioengineering, University of Washington, Seattle, Washington, United States
[3]School of Optometry and Vision Science Graduate Group, University of California, Berkeley, California, United States
[4]Francis I. Proctor Foundation, University of California, San Francisco, California, United States

Correspondence: Jacque L. Duncan, Department of Ophthalmology, University of California San Francisco, 10 Koret Way K113, San Francisco, CA 94143-0730, USA; jacque.duncan@ucsf.edu.

Submitted: June 13, 2018
Accepted: September 25, 2018

Citation: Qin J, Rinella N, Zhang Q, et al. OCT angiography and cone photoreceptor imaging in geographic atrophy. *Invest Ophthalmol Vis Sci*. 2018;59:5985–5992. https://doi.org/10.1167/iovs.18-25032

Purpose. To compare cone spacing and choriocapillaris (CC) perfusion adjacent to geographic atrophy (GA) in patients with age-related macular degeneration (AMD) and age-similar normal eyes.

Methods. Subjects were imaged using adaptive optics scanning laser ophthalmoscopy (AOSLO), fundus autofluorescence (FAF), and swept-source optical coherence tomography angiography. The GA border was identified using FAF images; CC flow void was analyzed in 1° regions extending from the GA border. A grader masked to CC perfusion selected regions of interest (ROIs) with unambiguous cone mosaics in AOSLO images. At each ROI, cone spacing and CC flow void were converted to Z-scores (standard deviations from the mean of 12 normal eyes aged 50 to 81 years for cone spacing, and 60 normal eyes age 51 to 88 years for CC flow void).

Results. Excluding regions of GA and drusen, CC flow void in eight eyes of six patients with AMD was significantly greater than in four age-similar normal eyes (exact permutation test, $P = 0.024$). CC flow void was negatively correlated with distance from the GA margin ($r = -0.35$; 95% confidence interval [CI], -0.53 to -0.12). Increased cone spacing was significantly correlated with CC flow void ($r = 0.33$; 95% CI, 0.12 to 0.59). Cone spacing was increased in 39% of ROIs, while CC flow void was increased in 96% of ROIs.

Conclusions. In eyes with GA due to AMD, CC hypoperfusion was significantly correlated with, and more extensive than, cone photoreceptor loss. The results suggest that reduced CC perfusion contributes to the development of GA.

Keywords: adaptive optics scanning laser ophthalmoscopy, geographic atrophy, swept source optical coherence tomography angiography

Age-related macular degeneration (AMD) is the leading cause of visual loss in elderly Americans.[1] Vision loss develops in patients who develop choroidal neovascularization and in patients with geographic atrophy (GA), when the atrophy involves fixation. GA occurs less commonly than choroidal neovascularization in AMD, but there are no effective treatments for GA, and eyes that develop GA have slightly lower visual acuity scores than those that develop neovascularization.[2] GA in AMD is characterized by loss of outer retinal cells in the macular region. Understanding the initial cause of GA may facilitate the development of clinical therapeutic strategies for the prevention of GA and subsequent vision loss in AMD. GA causes atrophy of the photoreceptors, retinal pigment epithelium (RPE), and choriocapillaris (CC), but it remains unclear whether the primary lesion involves cellular (RPE/photoreceptor) or vascular (CC) loss. Most attempts to develop therapies to prevent GA have focused on photoreceptor and RPE loss.[3,4] Phase 2 and 3 clinical trials targeted to RPE and photoreceptor preservation are ongoing (National Clinical Trial numbers 02659098, 03446144, 02686658, 02286089, 01782989, 02564978, 02684578, 02087085, and 02463344). However, an alternative theory posits that blood flow abnormalities play an important role in AMD based on deficiencies of choroidal blood flow in early and late AMD.[5,6] Histologic studies have identified reduced CC density at the edge of GA lesions in AMD patients,[7] and impaired CC perfusion may lead to impaired RPE function, degradation of photoreceptors, decreased antioxidant capacity, and increased drusen deposition.[7] CC loss is visible in early and intermediate stage AMD in histologic sections and is more advanced with increased AMD severity, suggesting that early CC loss could be a useful biomarker of the development and progression of GA.[7]

Understanding the cause of GA has been limited by the inability to obtain in vivo high-resolution images of photoreceptors, RPE, and CC perfusion in patients with AMD. Additionally, standard clinical imaging modalities, such as fluorescein and indocyanine green (ICG) angiography, fundus autofluorescence (FAF), and cross-sectional optical coherence tomography (OCT) B-scans lack the resolution necessary to characterize the earliest alterations in CC, photoreceptors, and RPE cells. Newer noninvasive imaging techniques for assessing CC perfusion and photoreceptors with cellular-level resolution in vivo may improve understanding of how GA develops. OCT-based angiography (OCTA) permits noninvasive, functional

imaging of retinal and choroidal vasculature[8–10] and has been used to visualize alterations in the CC of patients with dry AMD.[8] Swept-source OCT angiography (SS-OCTA), which features a high acquisition speed and an improved penetration depth, is a promising technology to provide insight into CC changes in GA.[8,11] Adaptive optics scanning laser ophthalmoscopy (AOSLO) enables direct visualization of waveguiding cone photoreceptors with cellular-level resolution, which permits quantitative measurements of changes in cone spacing or the average distance between neighboring cones.[12–14] Adaptive optics measure and compensate for aberrations in the optical path between the imaging camera and the retina.[12] AOSLO has been used to image retinal structures in AMD.[13,15,16] The combination of AOSLO and OCTA has the resolution to visualize macular photoreceptors and underlying CC perfusion in patients. We used these noninvasive, high-resolution retinal imaging techniques to compare cone photoreceptors and CC perfusion in regions bordering GA due to nonneovascular AMD with similar locations in normal eyes.

Materials and Methods

This study was approved by the Institutional Review Board of University of California, San Francisco, and informed consent was obtained from all subjects before performing study procedures. The study followed the tenets of the Declaration of Helsinki and was conducted in compliance with the Health Insurance Portability and Accountability Act. The clinical characteristics of the subjects studied are provided in the Table. All participants received comprehensive examinations of the anterior and posterior segments. Patients with AMD were considered for enrollment according to the following inclusion criteria: visual acuity >20/40, dry AMD with drusen >125-μm diameter, GA sparing the fovea, and no evidence of choroidal neovascularization or exudation in the study eye. The normal eyes were from age-similar subjects with visual acuity >20/40 in each eye and no AMD. All eyes studied had less than six diopters myopia and no other retinal vascular disease. Visual acuity was measured according to the Early Treatment of Diabetic Retinopathy Study (ETDRS) protocol with a measurement and correction of refractive error.[17] Imaging studies included color fundus photos (TRC 50DX; Topcon Medical Systems, Inc., Oakland, NJ, USA), axial length A scan measurements (IOL Master; Carl Zeiss Meditec, Dublin, CA, USA), cross-sectional spectral-domain OCT (SD-OCT) images including high resolution 20° horizontal and vertical B-scans, and 20° × 15° volume scans and FAF images (Spectralis HRA+OCT; Heidelberg Engineering, Vista, CA, USA). Regions of GA were outlined from areas of reduced autofluorescence in FAF images. Regions of increased backscatter with increased reflectance in infrared fundus images and SD-OCT images were used to confirm ambiguous areas of reduced autofluorescence in FAF images.

The custom-built AOSLO system used a low-coherence light source (NKT-EXR15; NKT Photonics, Inc., Denmark) with a central wavelength of 840 nm, a Shack-Hartmann wavefront sensor, and a 140-actuator microelectromechanical deformable mirror (Boston Micromachines Corporation, Watertown, MA, USA) as described previously.[13] The AOSLO montage covered areas of GA, adjacent borders of GA lesions, and CC normal-appearing regions for each subject.

An SS-OCTA system (PLEX Elite 9000; Carl Zeiss Meditec Inc.) was used for angiographic image acquisition, with a central wavelength of 1,060 nm and a speed of 100,000 A-scans per second. The axial and lateral resolutions of the system were ~5 μm in tissue and ~14 μm at the retinal surface. The scan pattern used in this study was 6 mm × 6 mm field of view, incorporating 500 B-scan positions in the slow axis, with each B-scan comprised of 500 A-scans (fast axis). At each B-scan position, the scanning was repeated twice to enable blood flow extraction by using the optical microangiography (OMAG) algorithm.[18] The scanning depth was 3 mm over 1536 pixels. A semiautomated segmentation algorithm was used to accurately identify the RPE/Bruch's membrane (BM) complex layer from the structural OCT volume derived from the OCTA dataset.[19] A slab starting from the outer boundary of BM to approximately 20 μm beneath BM was used to define the CC slab, upon which an algorithm was used to quantify the CC flow void, as previously described.[20] Briefly, this quantification algorithm first used the CC structural information to compensate for shadowing caused by the RPE and BM on the CC flow map, and then projection artifacts due to overlying retinal blood flow were removed using a previously described algorithm.[21] Finally, the percentage of CC with abnormally low flow (flow voids [FVs] or flow deficits) was calculated based on a thresholding strategy that defines abnormal CC flow at each pixel as one standard deviation below the mean flow signals obtained from a normative database of 20 young normal subjects with normal CC perfusion (aged from 20 to 39 years old).[20] One standard deviation was selected for FV identification because it has been validated to be reproducible and repeatable.[20] FV in each normal eye was compared at the same bands used to define regions extending from the margins of GA for each of the eight patient eyes, and the %FV values were averaged for each band in each normal eye to compare normal CC FV at the same locations as were measured in patients by using an exact permutation test. Lastly, a comparison of FV with cone spacing was performed using regions extending in 1° concentric bands centered on the foveal avascular zone in normal eyes. Within regions of GA, outlined based on FAF images, CC hypoperfusion was present, and large choroidal vessels were visible. Drusen were identified using an automated algorithm to segment a layer from the RPE to BM on the structural en face SS-OCT images.[20] Regions occupied by drusen and GA were excluded from calculations of CC flow void.[20]

Color fundus and FAF images were superimposed with vertical and horizontal SD-OCT B-scans, AOSLO montage images, and OCTA images by using retinal vascular landmarks. Regions near the edge of GA without drusen visible on OCT, color fundus photography, or FAF fundus images were selected for further analysis. Five regions extending in 1° bands from the GA borders were identified, in which quantitative CC flow void percentages were analyzed in patients with GA. To compare with the normal subjects, the five bands identified above were precisely overlaid onto the normal CC maps by using the central fovea as the reference. In this way, the CC flow void percentage evaluated from the concentric regions identified in GA subjects were compared with the spatial location-similar regions from the normal subject (Fig. 1B) and compared by using an exact permutation test (see below). An examiner (AR) masked to CC perfusion status selected 50 μm × 50 μm regions of interest (ROIs) in which unambiguous cone mosaics were visible in the AOSLO montages. Cone spacing was measured using custom software (Matlab, Natick, MA, USA) to derive a density recovery profile histogram,[22] as described previously.[23] Cone spacing varies with eccentricity from the fovea, so cone spacing values were converted to Z-scores, or number of standard deviations from the mean, based on a normative database of cone spacing measures in 12 normal eyes aged 50 to 81 years.[13] CC FVs were also converted to Z-scores based on a normative database of 60 eyes aged 51 to 89 years (mean, 69 years; standard deviation, 10 years). The Z-score is calculated as $Z_i = \frac{FVD_i - \overline{FVD}}{SD}$, where Z is Z-score, $\overline{FVD}$ and SD are the mean and standard deviation of flow void density (percentage; FVD)

Table. Clinical Characteristics of Subjects Studied

Subject	Eye	AOSLO ID	Age, y	Sex	AMD Classification*	Visual Acuity, Snellen Equivalent	Visual Acuity, ETDRS Letters Read
Patient 1 (P1)	Right	40120	83	M	Late AMD (GA)	20/25	83
Patient 1 (P1)	Left	40120	83	M	Late AMD (GA)	20/25	85
Patient 2 (P2)	Left	40118	75	F	Late AMD (GA)	20/32	78
Patient 3 (P3)	Left	40117	82	M	Late AMD (GA)	20/25	80
Patient 4 (P4)	Right	40124	84	M	Late AMD (GA)	20/30-2	78
Patient 5 (P5)	Right	40128	70	F	Late AMD (GA)	20/25	83
Patient 5 (P5)	Left	40128	70	F	Late AMD (GA)	20/25	83
Patient 6 (P6)	Right	40129	78	M	Late AMD (GA)	20/20	84
Normal 1 (N1)	Left	10021	79	M	No AMD	20/12	95
Normal 2 (N2)	Right	40119	57	M	No AMD	20/20	88
Normal 3 (N3)	Right	40171	81	F	No AMD	20/20	85
Normal 3 (N3)	Left	40171	81	F	No AMD	20/20	87

Y, years; M, male; F, female.

* AMD Classification is based on the Clinical Classification System for AMD, which is proposed by the Macular Research Classification Committee.[24] ETDRS, early treatment of diabetic retinopathy study.[17]

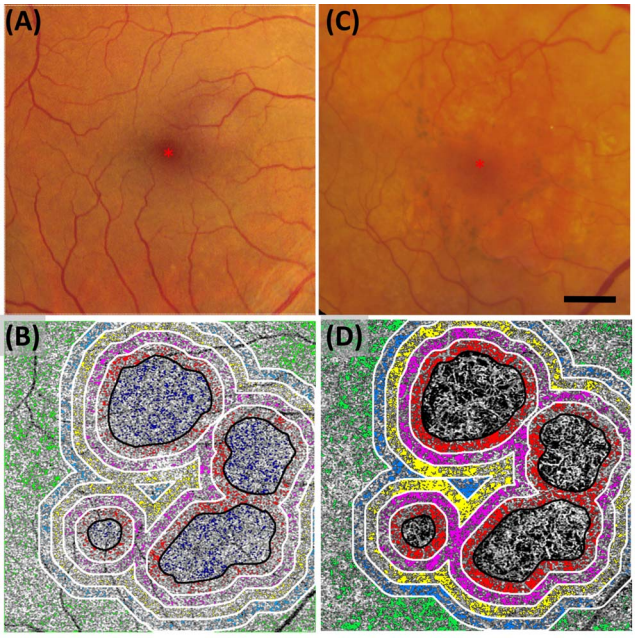

(E)

	Normal					GA (size = 6.74mm²)				
Degree	1st	2nd	3rd	4th	outside	1st	2nd	3rd	4th	outside
FVD	11.9%	11.8%	10.7%	10.4%	10.5%	41.5%	38.3%	35.4%	25.3%	19.6%
Z score	-0.36	-0.44	-1.09	-1.24	-1.19	17.24	15.34	13.61	7.60	4.21

Figure 1. Representative color fundus and OCTA images of normal subject N2, 40019R (**A**, **B**) and patient P5, 40128R (**C**, **D**). Color fundus photo of N2 (**A**) shows several patches of RPE depigmentation but no drusen were present on OCT B-scans, while P5 (**C**) shows drusen, areas of GA, and focal RPE hyperplasia. Color photos were scaled to match the 6 mm × 6 mm OCTA images in (**B**) and (**D**). FVs within five color coded regions that extend in 1° concentric bands from the margin of GA are overlaid onto the CC OCTA maps obtained from (**B**) normal and (**D**) GA subjects: 1st band, 0° to 1° (*red*); 2nd band, 1° to 2° (*magenta*); 3rd band, 2° to 3° (*yellow*); 4th band, 3° to 4° (*blue*); and outside, greater than 4° (*green*). GA regions are outlined in *black*. Colored pixels in (**B**) and (**D**) indicate regions of the CC flow void, defined as greater than 1 standard deviation below the mean of 20 normal subjects aged 20 to 39 years.[20] (**E**) CC flow void percentage across the bands and Z-scores for each of the 5 bands. *Red asterisks* show the foveal center; *scale bar*: 1 mm.

from normal database, respectively, and i indicates each eye. A lower Z-score means lower CC FVD, and a negative Z-score means FVDs below mean FVD of normal database. Normal Z-scores were between −2 and 2. Two standard deviations were used to evaluate how the FVD in the eye deviates from an age-similar normal population, as two is the standard threshold that has been commonly used to determine normal range.

Statistical Analysis

A permutation test was used to compare the difference of means in CC FVs between AMD patients and normal subjects. Spearman's rank correlation was used to compare cone spacing and CC flow void Z-scores at ROIs corresponding to regions with color-coded CC FVs at the margins of GA in AMD patients and in normal eyes at similar eccentricities. A bootstrap analysis, clustered by patient to account for the fact that one eye was used in some subjects and both eyes were used in others, was used to derive 95% CI values. Statistical significance was defined as $P < 0.05$ or 95% CI ranges that did not include zero.

Results

Clinical and imaging data were collected from eight eyes of six patients with GA and no evidence of neovascularization, and from two eyes of two age-similar normal subjects. Refractive error ranged from +3.50 to −1.50 spherical equivalents.

The vascular perfusion of the CC slabs in age-similar normal subjects showed a mean CC flow void of 12.53% ± 1.68% with a Z-score of 0.[20] An example of CC FVs in 1° bands extending from the fovea is shown in an age-similar normal subject and a patient with GA (Fig. 1). An assessment of concentric 1° bands surrounding the GA margin showed that CC flow void values were significantly greater than in normal eyes for all regions examined in all patients (exact permutation test, difference of means between AMD patients and normal subjects, $P = 0.024$). CC FVs were not significantly correlated with GA area (Spearman's rank correlation $r = -0.47$; 95% CI, −0.94 to 0.80), but CC flow void was negatively correlated with eccentricity from the GA margin (Spearman's rank correlation $r = -0.35$; 95% CI, −0.53 to −0.12) in AMD patients.

Figure 2 shows representative images of two eyes with GA acquired from multiple imaging modalities, incorporating color

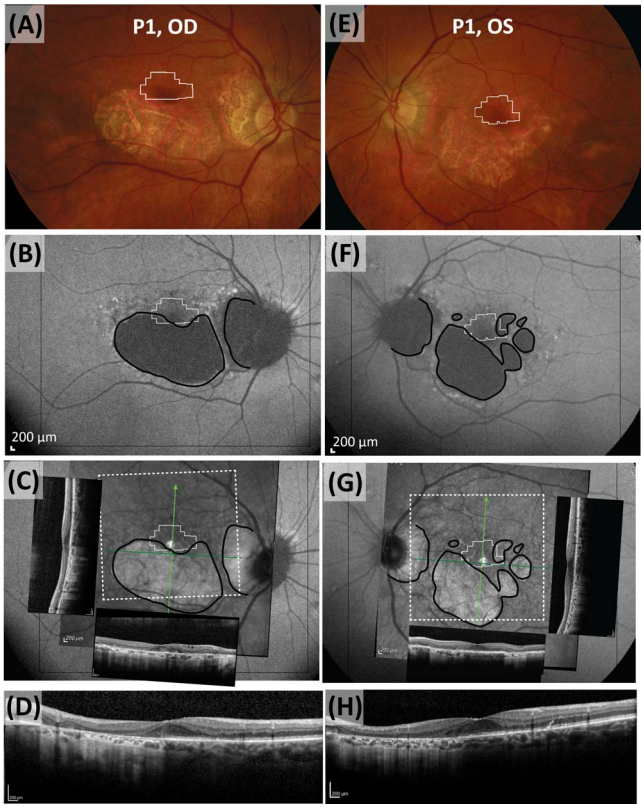

FIGURE 2. Representative multimodal images of GA in 2 eyes (P1, OU) with AMD. (**A**, **E**) Color fundus images of eyes with GA; *white solid lines* depict the area for AOSLO montage imaging. (**B**, **F**) FAF images; *black outlines* depict GA margins, and *white solid outlines* depict the area for AOSLO imaging. (**C**, **G**) FAF, near infrared, and SD-OCT. (**B**) Scan images were superimposed precisely; *green lines*, location of horizontal and vertical OCT cross-sectional B-scans; *white dotted lines* indicate the area for OCTA imaging. (**D**, **H**) Corresponding vertical OCT cross-sectional B-scans in **C**, **G**. Similar images are shown for patients P2 to P6 in Supplementary Figures S1 through S3. *Scale bars*: 200 µm.

fundus photos (Figs. 2A, 2E), FAF (Figs. 2B, 2F), and SD-OCT B-scans (Figs. 2C–H). The regions imaged with SS-OCTA (white dashed outline) and AOSLO (white solid outline) images were precisely superimposed and marked for comparisons between the cone mosaic and CC perfusion. GA areas appeared as sharply delineated regions of RPE loss in FAF fundus photos (Figs. 2B, 2F), whereas OCT B-scans show increased backscatter (Figs. 2C–H), which were marked by graders as black outlines as shown. The eyes shown in Figure 2 showed the lowest CC flow void percentages of all subjects studied and may represent the least abnormal example. Images of the other six eyes are shown in the supplementary Figures 1 through 3.

Figure 3 shows the representative OCTA CC images with AMD and AOSLO images with ROIs where cone spacing was measured. FVs were labeled with color-coded pixels overlaid with OCTA CC images (Figs. 3A, 3D). AOSLO images were precisely superimposed with OCTA CC images, with ROIs extending 50 µm × 50 µm (Figs. 3B, 3E). FVD and Z-scores were calculated for regions extending from the GA margin in concentric 1° color-coded bands, labelled 1st through 4th°, with outside representing the region greater than 4° from the GA margin (Figs. 3C, 3F). Results of the other six eyes are shown in Supplementary Figures S4 through S6.

Figure 4 shows representative cone spacing measurements at ROIs superimposed on the color-coded concentric 1° bands, shown as 5 bands extending from the GA margin. Cone spacing and CC flow void percentages in each 1° concentric band were calculated as Z-scores and compared with age-similar normal values.

Figure 5 shows cone spacing with respect to eccentricity for the ROIs in three age-similar normal eyes and all eight eyes with AMD. The majority (28/46, or 61%) of cone spacing values in eyes with GA fell within the 95% CIs around the normal mean and showed cone spacing Z-scores <2. However, 18/46, or 39%, of ROIs showed cone spacing values that were increased by greater than the 95% CIs, with cone spacing Z-scores >2. Cone spacing Z-scores were significantly and positively correlated with CC flow void Z-scores (Spearman's rank correlation rho = 0.33; 95% CI, 0.12 to 0.59). CC perfusion was abnormally reduced, with a CC flow void Z-score >2 in 44 of the 46 ROIs where cone spacing was measured in the eyes with AMD (Fig. 5, red squares). Only 2 of the 46 (4%) ROIs were located in regions with normal CC perfusion (CC flow void Z-score, <2), and in both of these ROIs, cone spacing fell within normal limits (Fig. 5, blue squares).

DISCUSSION

Reduced CC perfusion, represented by increased CC flow void, was correlated with increased cone photoreceptor spacing in eyes with nonneovascular AMD and fovea-sparing GA, suggesting that CC hypoperfusion accompanies cone loss. CC flow void was significantly correlated with increased cone spacing; there were regions with normal cone spacing in areas with reduced CC perfusion, but no regions with increased cone spacing in locations with normal CC perfusion (Fig. 5). Furthermore, CC flow void was significantly and negatively correlated with distance from the edge of GA. The data suggest that CC hypoperfusion was observed more commonly and more extensively than the loss of overlying cone photoreceptors and that CC hypoperfusion may precede RPE atrophy, GA enlargement, and cone photoreceptor loss. However, it is possible that cones have normal spacing but may have decreased function with reduced metabolic demand, resulting in reduced CC flow. Rods, which were not imaged in the current study, are lost and have impaired function in eyes with AMD,[25,26] and it is possible that rod loss may cause reduced CC flow despite normal cone spacing measures. Longitudinal studies of patients with AMD are necessary to establish the relationship between photoreceptor loss, CC flow void, and GA progression.

The CC flow void was significantly greater in the regions surrounding the margin of GA in the AMD patients than in normal eyes. This is similar to histologic studies that have shown CC loss even in early stages of AMD,[7] and OCTA may provide a sensitive method to measure the earliest CC perfusion changes in eyes with AMD. CC flow void throughout the 6 mm × 6 mm region showed diffuse CC flow abnormalities in eyes with GA due to AMD. In the current study, GA area was not significantly correlated with CC flow void, but this small study may have been insufficiently powered to detect a significant relationship between GA area and CC flow void.

The combination of AOSLO and OCTA imaging may shed new light on the mechanism of GA progression. GA area was defined by hypoautofluorescence by using FAF images as a surrogate for RPE cell survival, but RPE cells were not evaluated with resolution commensurate with the resolution of the AOSLO and OCTA systems used to study cone photoreceptors and CC perfusion, respectively. Images in the current manuscript were acquired using a confocal AOSLO system, in which white spots in a mosaic represent cones with

Investigative Ophthalmology & Visual Science

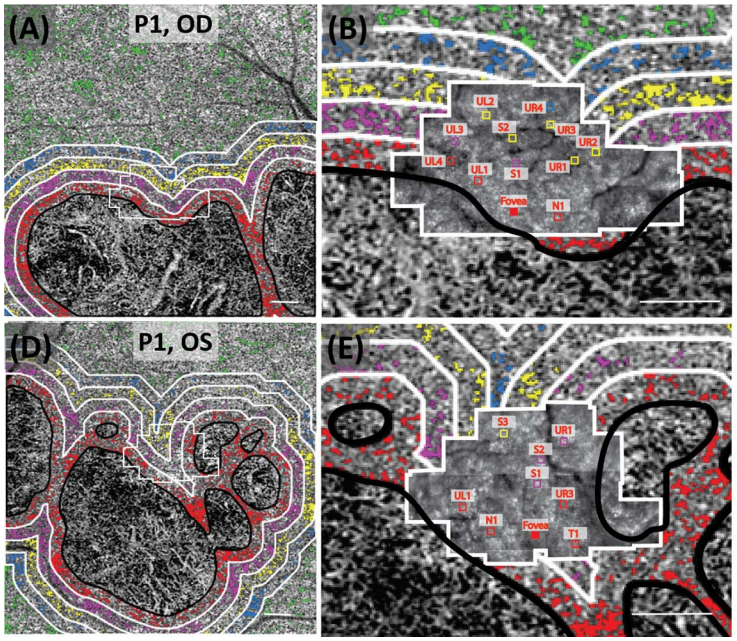

P1, OD		
GA size = 10.2 mm²		
Degree	FVD	Z-score
1st	27.0%	7.93
2nd	25.4%	5.58
3rd	21.6%	7.05
4th	13.3%	1.38
outside	5.65%	-4.32

P1, OS		
GA size = 10.5 mm²		
Degree	FVD	Z-score
1st	22.1%	5.13
2nd	16.9%	2.00
3rd	12.1%	0.32
4th	8.12%	-1.92
outside	4.62%	-5.22

Figure 3. Representative OCTA CC images in 2 eyes (P1, OU: OD, *top row*; and OS, *bottom row*) with AMD. The CC FVs are shown as colored pixels in regions extending from the GA margin in concentric 1° color-coded bands, labeled 1st to 4th°, with outside representing the region greater than 4° from the GA margin (*black outlines*), and AOSLO images with ROIs where cone spacing was measured. GA area and drusen were excluded from the CC flow void analysis. (**A**, **D**) CC images with color-coded FVs. (**B**, **E**) AOSLO images with ROIs extending 50 μm × 50 μm labeled with letters and numbers indicating relative position with respect to the fovea. UL, upper left; UR, upper right; LL, lower left; LR, lower right; N, nasal; T, temporal; S, superior; P, patient. *Scale bars*: 500 μm. (**C**, **F**) GA area, CC FVD, and Z-scores for each of the 5 regions extending from the GA margin as follows: 1st, 0° to 1° (*red*); 2nd, 1° to 2° (*magenta*); 3rd, 2° to 3° (*yellow*); 4th, 3° to 4° (*blue*); outside, greater than 4° (*green*) from the GA margin. Images from patients P2 OS and P3 OS are shown in Supplementary Figure S4, P4 OD and P5 OD in Supplementary Figure S5, and P5 OS and P6 OD are shown in Supplementary Figure S6.

intact inner and outer segments in contact with RPE cells.[27] Nonconfocal AOSLO systems can provide a high-quality visualization of cones that have inner segments but without intact outer segments,[28] and RPE cells can be imaged using split detection and dark field AOSLO systems.[29] Confocal images of RPE cells have been demonstrated using short-wavelength autofluorescence,[30–32] near-infrared autofluorescence,[15] two-photo autofluorescence in nonhuman primates,[33] and adaptive optics enhanced ICG.[34] Combined with confocal AOSLO imaging systems, nonconfocal AOSLO is capable of

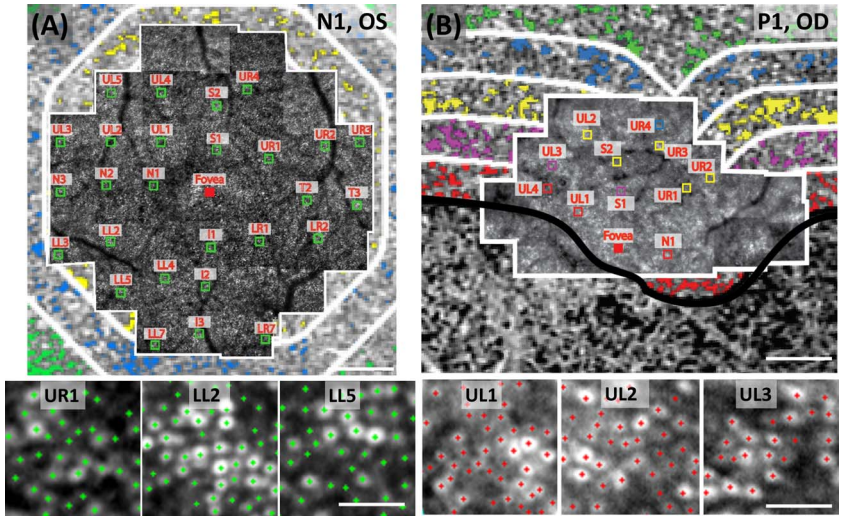

Figure 4. Representative AOSLO montages (outlined in *white*) superimposed on CC slab from OCTA images. (**A**) Normal subject N1 (10021L); (**B**) patient P1 (40120R) with GA. *Green squares* (50 μm ×50 μm) in **A** show ROIs where cones were unambiguously seen and counted. Green crosses in enlarged insets (UR1, LL2, and LL5) in the bottom of **A** show examples of cone selections. In **B**, the *square insets* (50 μm × 50 μm) are color coded with each of the five concentric regions extending from the GA margin as follows: 1st, 0° to 1° (*red*); 2nd, 1° to 2° (*magenta*); 3rd, 2° to 3° (*yellow*); 4th, 3° to 4° (*blue*); outside, greater than 4° from the GA margin (*green*). (**B**) CC FVs are shown for each band. UL, upper left; UR, upper right; LL, lower left; LR, lower right. UL1, UL2, and UL3 are enlarged at *bottom* to show cone markings; UR1 versus UL1, LL2 versus UL2, and LL5 versus UL3 were selected for comparison of ROIs at similar eccentricities. *Scale bars*: 500 μm (large montages) and 50 μm (magnified insets). Images of P1 OS, P2 OS, P3 OS, P4 OD, P5 OD, P5 OS, and P6 OD with representative ROIs are shown in Supplementary Figure S7.

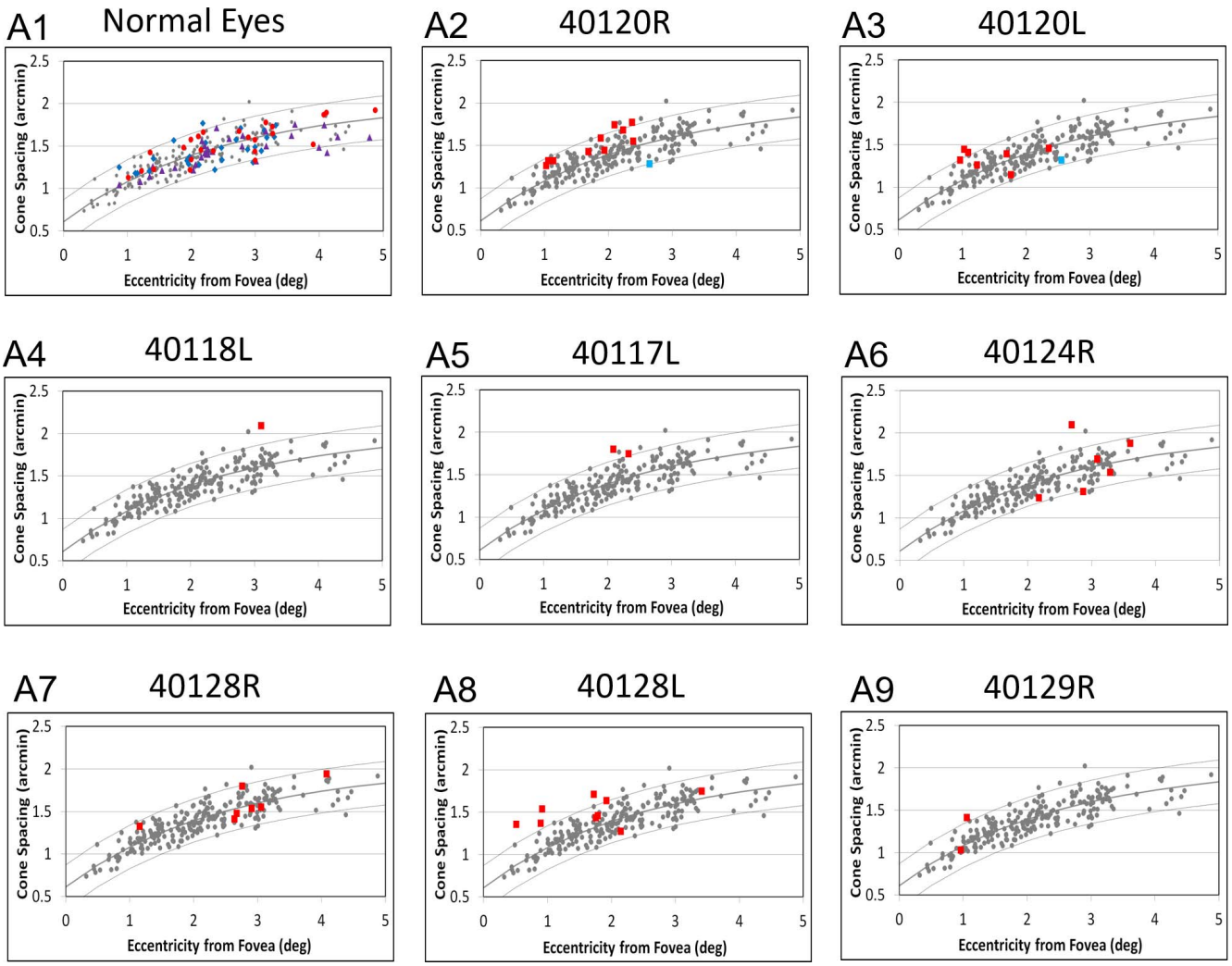

Figure 5. (**A1–A9**) CC flow void is abnormal in most ROIs, even those with normal cone spacing. (**A1**) Cone spacing measurements in age-similar normal eyes. *Small gray dots* in **A1–A9**, cone spacing measures of 12 age-similar (50 to 81 years old) normal subjects[13]; *dark solid lines*, mean normal data; *upper* and *lower gray curves*, 95% confidence limits; *blue diamonds*, N1 (10021L); *purple triangles*, N2 (40119R); and *red circles*, N3 (40171L). All cone spacing measures in 10021L, 40119R, and 40171L were in regions with CC FVs that showed Z-scores <2. (**A2–A9**) Cone spacing measurements as a function of eccentricity from the foveal center in AMD patients with GA. *Red squares*, cone spacing in regions with increased CC flow void (Z-score ≥2); *blue squares*, cone spacing in regions with normal CC flow void (Z-score <2).

providing insight into the progression of photoreceptor and RPE loss and may be useful for monitoring the effects of treatments designed to control or slow the progression of retinal and choroidal diseases. Future studies combining confocal and nonconfocal AOSLO with OCTA images may provide further insight into cellular mechanisms of disease progression in eyes with AMD by demonstrating individual RPE cells. These studies might also expedite the development and assessment of therapies to prolong photoreceptor and CC survival. In addition, future research will study patients longitudinally to monitor eyes for GA progression. A more complete understanding of microvascular dynamics and changes in cone photoreceptors may enhance our understanding of the pathophysiology of GA in AMD patients.

Most current clinical trials to treat GA have been directed at photoreceptor[3] or RPE[4] degeneration or inflammatory mechanisms mediated through the alternate complement pathway.[35] Although several studies have investigated CC perfusion in eyes with GA due to AMD,[5,6,36] the advent of OCTA makes it much easier to investigate the relationship between CC perfusion and GA progression. If longitudinal studies demonstrate a correlation between CC FVs and increased risk of GA progression, therapies to address impaired blood supply to the outer retina in patients with AMD may reduce the risk of GA progression and vision loss. Here, we have demonstrated that CC alterations correlate with cone photoreceptor abnormalities, as CC FVs were associated with increased cone spacing. These findings suggest that impaired CC perfusion may contribute to GA development and photoreceptor loss. Future prospective, longitudinal studies of CC perfusion and cone survival in eyes with AMD and GA may demonstrate whether CC perfusion abnormalities precede or predict future cone loss and GA progression.

Acknowledgments

Supported by NIH Grants NIH EY002162, EY 024239, EY024158, and FDA R01-41001; Research to Prevent Blindness; The Bernard A. Newcomb Macular Degeneration Fund; That Man May See, Inc.; Hope for Vision; Foundation Fighting Blindness; Beckman Initiative for Macular Research Grant 1201; The Claire Giannini Fund; L.L. Hillblom Foundation Research Network Grant; The Hedco

Foundation; and The Pritzker Foundation. An NEI ARVO Travel Award provided support to present some of the results at the annual ARVO meeting in Baltimore, MD.

Disclosure: **J. Qin**, None; **N. Rinella**, None; **Q. Zhang**, None; **H. Zhou**, None; **J. Wong**, None; **M. Deiner**, None; **A. Roorda**, P; **T.C. Porco**, None; **R.K. Wang**, Research to Prevent Blindness (F), Carl Zeiss Meditec (C), Insight Photonic Solutions (C), P; **D.M. Schwartz**, P; **J.L. Duncan**, Neurotech USA (F), Second Sight Medical Products, Inc. (F), Allergan (F), NightStar, Inc. (F), AGTC (C), Editas (C), ProQR (C, R), Sparing Vision (C), Spark Therapeutics (C)

References

1. Klein R, Klein BE, Knudtson MD, Meuer SM, Swift M, Gangnon RE. Fifteen-year cumulative incidence of age-related macular degeneration: the Beaver Dam Eye Study. *Ophthalmology*. 2007;114:253–262.
2. Chew EY, Clemons TE, Agron E, et al. Ten-year follow-up of age-related macular degeneration in the age-related eye disease study: AREDS report no. 36. *JAMA Ophthalmol*. 2014;132:272–277.
3. Zhang K, Hopkins JJ, Heier JS, et al. Ciliary neurotrophic factor delivered by encapsulated cell intraocular implants for treatment of geographic atrophy in age-related macular degeneration. *Proc Natl Acad Sci U S A*. 2011;108:6241–6245.
4. Schwartz SD, Regillo CD, Lam BL, et al. Human embryonic stem cell-derived retinal pigment epithelium in patients with age-related macular degeneration and Stargardt's macular dystrophy: follow-up of two open-label phase 1/2 studies. *Lancet*. 2015;385:509–516.
5. Grunwald JE, Hariprasad SM, DuPont J, et al. Foveolar choroidal blood flow in age-related macular degeneration. *Invest Ophthalmol Vis Sci*. 1998;39:385–390.
6. Pauleikhoff D, Chen JC, Chisholm IH, Bird AC. Choroidal perfusion abnormality with age-related Bruch's membrane change. *Am J Ophthalmol*. 1990;109:211–217.
7. Seddon JM, McLeod DS, Bhutto IA, et al. Histopathological insights into choroidal vascular loss in clinically documented cases of age-related macular degeneration. *JAMA Ophthalmol*. 2016;134:1272–1280.
8. Moult EM, Waheed NK, Novais EA, et al. Swept-source optical coherence tomography angiography reveals choriocapillaris alterations in eyes with nascent geographic atrophy and drusen-associated geographic atrophy. *Retina*. 2016;36(Suppl 1):S2–S11.
9. Schwartz DM, Fingler J, Kim DY, et al. Phase-variance optical coherence tomography: a technique for noninvasive angiography. *Ophthalmology*. 2014;121:180–187.
10. Chen CL, Wang RK. Optical coherence tomography based angiography [Invited]. *Biomed Opt Express*. 2017;8:1056–1082.
11. Lains I, Wang J, Providencia J, et al. Choroidal changes associated with subretinal drusenoid deposits in age-related macular degeneration using swept-source OCT. *Am J Ophthalmol*. 2017;180:55–63.
12. Roorda A, Romero-Borja F, Donnelly W III, Queener H, Hebert T, Campbell M. Adaptive optics scanning laser ophthalmoscopy. *Opt Express*. 2002;10:405–412.
13. Zayit-Soudry S, Duncan JL, Syed R, Menghini M, Roorda AJ. Cone structure imaged with adaptive optics scanning laser ophthalmoscopy in eyes with nonneovascular age-related macular degeneration. *Invest Ophthalmol Vis Sci*. 2013;54:7498–7509.
14. Zayit-Soudry S, Sippl-Swezey N, Porco TC, et al. Repeatability of cone spacing measures in eyes with inherited retinal degenerations. *Invest Ophthalmol Vis Sci*. 2015;56:6179–6189.
15. Rossi EA, Rangel-Fonseca P, Parkins K, et al. In vivo imaging of retinal pigment epithelium cells in age related macular degeneration. *Biomed Opt Express*. 2013;4:2527–2539.
16. Zhang Y, Wang X, Godara P, et al. Dynamism of dot subretinal drusenoid deposits in age-related macular degeneration demonstrated with adaptive optics imaging. *Retina*. 2017;38:29–38.
17. Ferris FL III, Kassoff A, Bresnick GH, Bailey I. New visual acuity charts for clinical research. *Am J Ophthalmol*. 1982;94:91–96.
18. Wang RK, Zhang A, Choi WJ, et al. Wide-field optical coherence tomography angiography enabled by two repeated measurements of B-scans. *Opt Lett*. 2016;41:2330–2333.
19. Yin X, Chao JR, Wang RK. User-guided segmentation for volumetric retinal optical coherence tomography images. *J Biomed Opt*. 2014;19:086020.
20. Zhang Q, Zheng F, Motulsky EH, et al. A novel strategy for quantifying choriocapillaris flow voids using swept-source OCT angiography. *Invest Ophthalmol Vis Sci*. 2018;59:203–211.
21. Zhang A, Zhang Q, Wang RK. Minimizing projection artifacts for accurate presentation of choroidal neovascularization in OCT micro-angiography. *Biomed Opt Express*. 2015;6:4130–4143.
22. Rodieck RW. The density recovery profile: a method for the analysis of points in the plane applicable to retinal studies. *Vis Neurosci*. 1991;6:95–111.
23. Duncan JL, Zhang Y, Gandhi J, et al. High-resolution imaging with adaptive optics in patients with inherited retinal degeneration. *Invest Ophthalmol Vis Sci*. 2007;48:3283–3291.
24. Ferris FL III, Wilkinson CP, Bird A, et al. Clinical classification of age-related macular degeneration. *Ophthalmology*. 2013;120:844–851.
25. Curcio CA, Medeiros NE, Millican CL. Photoreceptor loss in age-related macular degeneration. *Invest Ophthalmol Vis Sci*. 1996;37:1236–1249.
26. Owsley C, McGwin G Jr, Jackson GR, Kallies K, Clark M. Cone- and rod-mediated dark adaptation impairment in age-related maculopathy. *Ophthalmology*. 2007;114:1728–1735.
27. Putnam NM, Hammer DX, Zhang Y, Merino D, Roorda A. Modeling the foveal cone mosaic imaged with adaptive optics scanning laser ophthalmoscopy. *Opt Express*. 2010;18:24902–24916.
28. Scoles D, Sulai YN, Langlo CS, et al. In vivo imaging of human cone photoreceptor inner segments. *Invest Ophthalmol Vis Sci*. 2014;55:4244–4251.
29. Scoles D, Sulai YN, Dubra A. In vivo dark-field imaging of the retinal pigment epithelium cell mosaic. *Biomed Opt Express*. 2013;4:1710–1723.
30. Morgan JI, Dubra A, Wolfe R, Merigan WH, Williams DR. In vivo autofluorescence imaging of the human and macaque retinal pigment epithelial cell mosaic. *Invest Ophthalmol Vis Sci*. 2009;50:1350–1359.
31. Morgan JI, Hunter JJ, Masella B, et al. Light-induced retinal changes observed with high-resolution autofluorescence imaging of the retinal pigment epithelium. *Invest Ophthalmol Vis Sci*. 2008;49:3715–3729.
32. Morgan JI, Hunter JJ, Merigan WH, Williams DR. The reduction of retinal autofluorescence caused by light exposure. *Invest Ophthalmol Vis Sci*. 2009;50:6015–6022.
33. Sharma R, Williams DR, Palczewska G, Palczewski K, Hunter JJ. Two-photon autofluorescence imaging reveals cellular structures throughout the retina of the living primate eye. *Invest Ophthalmol Vis Sci*. 2016;57:632–646.
34. Tam J, Liu J, Dubra A, Fariss R. In vivo imaging of the human retinal pigment epithelial mosaic using adaptive optics

Investigative Ophthalmology & Visual Science

enhanced indocyanine green ophthalmoscopy. *Invest Ophthalmol Vis Sci*. 2016;57:4376–4384.

35. Yaspan BL, Williams DF, Holz FG, et al. Targeting factor D of the alternative complement pathway reduces geographic atrophy progression secondary to age-related macular degeneration. *Sci Transl Med*. 2017;9:eaaf1443.
36. Coleman DJ, Silverman RH, Rondeau MJ, Lloyd HO, Khanifar AA, Chan RV. Age-related macular degeneration: choroidal ischaemia? *Br J Ophthalmol*. 2013;97:1020–1023.

Investigative Ophthalmology & Visual Science